The Pacific Decadal Precession and its Relationship to Tropical Pacific Decadal Variability in CMIP6 Models

Matthew H. Rogers (rawrgers@uw.edu)
UW Climate Impacts Group https://orcid.org/0000-0003-4587-189X
Jason Furtado
University of Oklahoma Norman Campus: The University of Oklahoma
Bruce Anderson
Boston University

Research Article

Keywords: Climate Dynamics, Pacific Variability, ENSO, Tropical Pacific Decadal variability, Pacific Decadal Precession

Posted Date: November 9th, 2021

DOI: https://doi.org/10.21203/rs.3.rs-390152/v1

Climate Dynamics manuscript No.
(will be inserted by the editor)

The Pacific Decadal Precession and its relationship to Tropical Pacific Decadal Variability in CMIP6 models

Matthew H. Rogers · Jason C. Furtado · Bruce T. Anderson

Received: date / Accepted: date

Abstract Persistent, multi-year shifts in atmospheric circulations and their associated influence on regional climates have profound impacts on physical, biological, and socioeconomic systems. The Pacific Decadal Precession (PDP), an atmospheric mode of variability consisting of a lower tropospheric height dipole which rotates counterclockwise over several years in the North Pacific, describes a series of such shifts in atmospheric circulations. One phase of the PDP, the north-south (N-S) phase, is hypothesized to be partially driven by central tropical Pacific (CP) sea surface temperature (SST) variability, but robust assessment of this dynamical connection in climate models remains to be done. In this study, we investigate this hypothesis with analyses in both reanalysis and selected models from the Coupled Model Intercomparison Project Phase 6 (CMIP6) archive. We show that the emergence of the N-S phase is both related to and influenced by tropical Pacific decadal SST variability, specifically variability associated with CP El Niño-Southern Oscillation (ENSO) events. When examining the pre-industrial runs of the CMIP6 models, we find that most models cannot recover the characteristic cyclonic precession of the dipoles of the PDP, instead featuring only amplitude and sign changes of the N-S phase, Moreover, the models do not replicate the dynamical connections between the tropical Pacific and this North Pacific mode of climate variability. Our results suggest that primary reasons for this inconsistency are that models inaccurately simulate both the SST pattern associated with the PDP, shared low-frequency power associated with CP ENSO events, and incorrect Rossby wavetrains emanating from the tropical Pacific into the North Pacific on quasi-decadal timescales. Taken together, our analyses offer another benchmark by which to test the fidelity of the climate model simulations in capturing Pa-

Matthew H. Rogers
Climate Impacts Group, The University of Washington, Seattle, WA, USA
Tel.: 206-616-6865
E-mail: rawrgers@uw.edu

Jason C. Furtado
School of Meteorology, The University of Oklahoma, Norman, OK, USA

Bruce T. Anderson
Department of Earth and Environment, Boston University, Boston, MA, USA

cific decadal climate variability in order to improve decadal-to-centennial climate projections.

Keywords Climate Dynamics · Pacific Variability · ENSO · Tropical Pacific Decadal variability · Pacific Decadal Precession

Declarations

Funding: Not applicable

Conflicts of interest/Competing interests: None

Availability of data and material: 20th Century Reanalysis V2c data are provided by the NOAA/OAR/ESRL PSL, Boulder, Colorado, USA, and are publicly available at `https://psl.noaa.gov/`. The Hadley Centre's Ice and Sea Surface Temperature (HadISST) data are publicly available for free download from the Met Office Hadley Centre at `https://www.metoffice.gov.uk/hadobs/hadisst/data/download.html`. The model output from the Coupled Model Intercomparison Project Phase 6 (CMIP6) are publicly available for download (upon free registration) from the Earth System Grid Federation (ESGF) at `https://esgf.llnl.gov/`.

Code availability: All analyses were conducted using Python. Code for analyses are available from the corresponding author upon request.

Authors' contributions: M. H. Rogers and J. C. Furtado conducted the data analysis for the manuscript. All authors contributed to the writing and editing of the manuscript.

1 Introduction

Large-scale climate variations, like those associated with the North Pacific Oscillation (NPO; e.g., Rogers, 1981) and the Pacific Decadal Oscillation (PDO; Mantua et al, 1997), have been linked to significant regional climate shifts in the North Pacific. Examples of such shifts include persistent drought in California (e.g., Diffenbaugh et al, 2015; Cook et al, 2018), anomalously warm sea surface temperatures (SSTs) in the Gulf of Alaska (e.g., Bond et al, 2015; Di Lorenzo and Mantua, 2016), and the disruption of marine ecosystems in the Pacific (Mantua et al, 1997; Di Lorenzo et al, 2008; Litzow et al, 2020; Cheung and Frölicher, 2020). The severity of these impacts has motivated considerable research into the dynamics and impacts of these modes of variability in the Pacific (Rogers, 1981; Mantua et al, 1997; Newman et al, 2003; Duffy et al, 2005; Schneider and Cornuelle, 2005; Di Lorenzo et al, 2008,0; Newman et al, 2016). Currently, two paradigms exist through which the research community views Pacific variability: **(1)** the *leading mode paradigm*, which includes interactions between the El Niño - Southern Oscillation (ENSO), the Aleutian Low, and the PDO; and **(2)** the *secondary mode paradigm*, consisting of Central Pacific (CP) ENSO, the NPO, and the North Pacific Gyre Oscillation (NPGO; Di Lorenzo et al, 2008). Understanding the dynamics of Pacific climate variability has proven difficult, as the interactions between various modes of variability in both the tropics and extratropics are complex and occur over multiple timescales (e.g., Pierce et al, 2001; Deser et al, 2017; Zhang et al, 2018b; Capotondi et al, 2018; Sun and Okumura, 2019). Still, efforts to isolate the contributions of several of these modes of variability and their feedbacks have improved (sub-)seasonal forecasts both globally and regionally (e.g., Goddard and Dilley, 2005; Zhang, 2005; Moore, 2012; Cox et al, 2019; Jacox et al, 2020). Advances made in our understanding of natural variability in the Pacific are useful in mitigating physical, biological, and economic impacts from regional climate shifts both presently and under future climate change.

The mechanisms that drive the ENSO-AL-PDO paradigm are well studied (e.g., Diaz et al, 2001; Alexander et al, 2002; Kwon and Deser, 2007; Shakun and Shaman, 2009; Wang et al, 2012; Wang, 2018; Zhang et al, 2018b; Wills et al, 2019). Less understood are the mechanisms driving and impacts of the CP ENSO-NPO-NPGO paradigm. Consideration of these secondary modes of variability is needed for a more complete understanding of Pacific variability and seasonal conditions experienced in North America. For example, Baxter and Nigam (2015) concluded that the NPO, a north-south oriented dipole in sea level pressure anomalies across the North Pacific, was the primary contributor to extreme winter weather across the midwestern United States during the winter of 2013-2014. Moreover, Hartmann (2015) tied anomalous ridging in the Gulf of Alaska, responsible for another extreme winter across central and eastern North America during 2014-15, to remote forcing from tropical convection and specifically weak CP ENSO-like conditions during that period. This remote forcing also likely reinforced the "Warm Blob" signature (i.e., persistently warm SST anomalies (SSTa) in the North Pacific) for that winter (Bond et al, 2015). Because of these events and others, researchers have recently investigated mechanisms of the secondary paradigm of Pacific variability and their impact on quasi-decadal North Pacific and North American climate variability (e.g., Liu and Di Lorenzo, 2018; Sun and Okumura, 2019).

The coauthors of this work have recently advanced knowledge of the secondary mode paradigm by identifying another mode of atmospheric variability in the North Pacific tied directly to hydrometeorology in the Northwestern US: the Pacific Decadal Precession (PDP; Anderson et al, 2016). While most modes of atmospheric climate variability are considered stationary patterns (e.g., the Aleutian Low, the NPO), the PDP is characterized by a cyclonically-propagating lower-tropospheric anomalous pressure dipole around the North Pacific during boreal winter, with a full revolution occurring over ∼12 years (Anderson et al, 2016). Figure 1 presents the full evolution of the PDP using 20$^{\text{th}}$ Century Reanalysis version 2c (Compo et al, 2011). The PDP is composed of two distinct phases, defined by the orientation of the dipole: a *north-south (N-S) phase* (Figs. 1a,b,e,f), when the pressure anomaly dipole is oriented meridionally, and an *east-west (E-W) phase* (Figs. 1c,d) when the dipole is oriented zonally. Signs of precession can be seen throughout the series of maps, with the positive anomaly comprising the northern pole of the PDP at Year -2 (Fig. 1a) rotating counter-clockwise to become the western pole at Year 0 (Fig. 1c) and the southern pole at Year +2 (Fig. 1e). The evolution of the PDP results in changes in atmospheric circulation over the North Pacific which consequently impact precipitation and temperature conditions downstream across North America because of associated changes in the jet stream (Anderson et al, 2016). These patterns are both unique and poorly related to the leading modes of Pacific variability (e.g., Anderson et al, 2016), further justifying the importance of the secondary mode paradigm within the large context of Pacific climate variability.

Previous studies on the PDP showed statistical evidence of the structure of the PDP and associated lagged teleconnections in regional climate. However, the dynamics of the PDP, including what forcings are responsible for the unique propagation of this mode, remain unknown. Potential drivers of the PDP are briefly discussed in Anderson et al (2016) and include: **(1)** The N-S phase is driven by teleconnections from the central tropical Pacific; and **(2)** The E-W phase is driven by stratospheric temperature deviations through their influence on underlying tropospheric circulations. This study focuses on the first hypothesis regarding the N-S phase of the PDP. Motivation for Hypothesis #1 primarily relies on the connection between the N-S phase of the PDP and the NPO (Fig 1; Anderson et al, 2017), implying that the PDP lies within the CP ENSO-NPO-NPGO paradigm. Prior studies have quantified the role of the tropical Pacific in driving seasonal-to-decadal variability in the NPO. Di Lorenzo et al (2010) and Furtado et al (2012) used modeling experiments to illustrate that the low-frequency variability in the NPO, particularly its southern node, lies in central tropical Pacific SST variability. Similar results were found by Yeh et al (2018), who tied late 20$^{\text{th}}$ century trends in the NPO to changes in tropical Pacific convection. Sung et al (2019) illustrated that variations in the position and strength of the NPO, and its downstream impacts on North American winters, are related to tropical Pacific SSTs and tropical convective patterns. Therefore, while previous research supports this hypothesis, a formal analysis investigating a dynamical relationship between CP ENSO and the N-S phase of the PDP has yet to be conducted in reanalysis data or model output.

Though research on the PDP has primarily used reanalysis data, identification and testing of the mechanisms associated with the PDP require us to look at atmosphere-ocean coupled general circulation models (AOGCMs). Historically,

however, AOGCMs have not performed well in simulating Pacific variability on multiple spatio-temporal scales, with previous studies showing a wide range in fidelity for modes like ENSO (Kim and Yu, 2012; Deser et al, 2017; Yim et al, 2015) and the NPO (Furtado et al, 2011). The connections between these modes of variability are weak and even non-existent in some AOGCMs (Furtado et al, 2011; Deser et al, 2012), especially on the quasi-decadal time scale, such that previous studies have drastically increased forcings artificially to ensure a robust atmospheric response (e.g., Shi et al, 2019). How AOGCMs simulate Pacific decadal climate variability present a significant barrier for skillful predictions of these modes and in understanding how Pacific variability may change under a warming climate (Yeh et al, 2009; Di Lorenzo et al, 2010; Furtado et al, 2011; Liu and Di Lorenzo, 2018).

This study seeks to expand our knowledge of how the latest climate models in the Coupled Model Intercomparison Project, Phase 6 (CMIP6) model archive (Eyring et al, 2016) simulate the PDP and its dynamical connections. The guiding hypotheses for this study are (a) The N-S phase of the PDP is linked to tropical Pacific decadal variability and, specifically, quasi-decadal variations in central tropical Pacific SSTs (i.e., variability associated with CP ENSO); and (b) only some AOGCMs will show evidence of relationships between the N-S phase of the PDP, the NPO, and Pacific decadal variability, particularly in the tropical Pacific. Through statistical analyses with available reanalysis and CMIP6 model output, we will provide a comprehensive picture of how well the selected models simulate the PDP and its hypothesized dynamical drivers. Altogether, our analyses will offer potential steps toward benchmarking another important mode of Pacific climate variability for future works.

2 Data and Methods

Observation-based atmospheric data are taken from 20^{th} Century Reanalysis version 2c (Compo et al, 2011). Specific atmospheric variables examined are monthly-mean geopotential height (on 24 pressure levels ranging non-uniformly from 1000 hPa to 10 hPa) and SLP on a 2° x 2° latitude by longitude grid over the period 1870–2013. SST data are taken from Hadley Centre's Ice and Sea Surface Temperature (HadISST) data set (Rayner et al, 2003), consisting of monthly-mean fields from 1870–near present on a 1°x1° latitude by longitude grid. Reanalysis variables from both datasets are considered over the common period 1870–2013. For CMIP6 model output, we use 300 years of pre-industrial control simulations (i.e., in which atmospheric CO_2 concentrations are held to pre-industrial levels so as to eliminate effects of anthropogenic influences on climate). The grid spacing for model output varies by both model and variable. To facilitate comparisons with our analyses of model output and reanalysis products, model SST data are regridded to a common 1° x 1° latitude by longitude grid, and the model atmospheric fields (i.e., geopotential height data and SLP) are regridded to the same 2° x 2° latitude by longitude grid as the reanalysis, both via bilinear interpolation. More detailed information on the model output used in this study is shown in Table 1.

All data have the long-term monthly-mean removed, and reanalysis data are linearly detrended to remove any potential anthropogenic influence on the variables prior to any statistical analyses. We also consider variables only during the

extended boreal cold season (i.e., November to March; NDJFM) and averaged over that season for seasonal means. The choice of NDJFM reflects the fact that the PDP and its individual phases are most active during this season (Anderson et al, 2016). Statistical significance of regression and correlation coefficients are determined via a bootstrapping method with 5000 iterations with replacement. For each of the 5000 iterations, one time series is randomized prior to the regression/correlation calculation. The compilation of these iterations create a distribution against which the true values are tested at the desired confidence level. Any data or model output that is described as "filtered" means it is subjected to an identical 7-20 year^{-1} Butterworth band-pass filter.

In both reanalysis and models, the PDP is defined using the procedures from Anderson et al (2017) briefly outlined below. Monthly mean NDJFM-averaged 850 hPa geopotential height anomalies over the North Pacific (15−80°N, 125°E-90°W) are band-pass filtered from 7-20 years^{-1} and then subjected to empirical orthogonal function (EOF) analysis. The leading mode (i.e., the pattern associated with low-frequency variability of the Aleutian Low) is then linearly removed from the height field via linear regression so that we can examine the quasi-decadal variability of the residuals. The residual spatio-temporal matrix is extended by 5 one-year lags prior to employ time-extended EOF analysis, which is a preferred method for identifying propagating modes of variability (e.g., the Madden-Julian Oscillation (MJO)). Regressing the filtered anomaly field onto the leading principal component time series from the time-extended EOF at the appropriate lags yields a sequence of 6 maps representing the progression of the PDP over a 6 year period. Following Anderson et al (2017), the third map in this series (i.e., Year 0) is designated as the central map, with the first two maps "leading" and last three maps "lagging" it. The leading principal component time series is hereafter referred to as the PDP index.

For diagnosing connections between the North Pacific and the tropical Pacific, we focus on ENSO variability and its flavors, namely eastern Pacific (or canonical) and CP ENSO. The canonical and CP ENSO structures are defined using the EOF-based approach outlined by Kim and Yu (2012). For the canonical ENSO mode, we linearly remove the influence from SSTa in the Niño-4 region (5°S-5°N, 160°E-150°W) from the full SSTa field for lags -3 to +3 months. After performing EOF analysis on the residuals over the domain 30°S-30°N, 120°E-60°W, the leading EOF is then multiplied by the square root of the associated eigenvalue to acquire the SSTa structure of canonical ENSO. The same techniques are applied to isolate SSTa associated with CP ENSO events, except the influence from the Niño1+2 region (10°S - 0°, 90°W-100°W) is linearly removed from the subtropical and tropical Pacific SSTa field instead of the Niño-4 region. The associated leading principal component time series of the EOF analyses provides an index tracking the canonical ENSO and CP ENSO phenomena.

Power spectrum analyses are also conducted on tropical Pacific SSTa indices in order to assess their dominant timescales of variability. Each time series is split in half, with one overlapping segment, yielding three (3) samples for power spectral analysis that are averaged together. A Hanning window is also appled to each segment prior to spectral decomposition. We use chi-squared testing and *a priori* statistics to assess the significance ($p < 0.05$) of the peaks in the power spectra. Use of *a priori* statistics is warranted as past studies have highlighted that the

canonical and CP ENSO phenomenon have power on interannual to decadal time scales (Diaz et al, 2001; Furtado et al, 2012; Wang, 2018)

3 Results

3.1 The PDP Structure in the CMIP6 Models

We begin our study by assessing the representation of the PDP in both the CMIP6 models and reanalysis data (Figure 2). In general, the CMIP6 models used in this study capture the general structure of the N-S phase of the PDP adequately (Figs. 2a, b, e, f; Years -2, -1, 2, 3), though the location, extent, and magnitude of the anomaly dipole vary across models. For example, the northern pole of the PDP in GISS-E2-1-G is larger in magnitude and situated farther west than in reanalysis (Fig. 2, Year 2). CESM2 simulates the northern pole of the N-S phase of the PDP with a northwesterly extension of the anomaly not seen in reanalysis, while MIROC6 simulates a pattern situated too far to the southeast. However, the biggest flaw with the simulated PDP in the models is that they do not accurately capture the E-W phase of the PDP. Only ACCESS-CM2 and CanESM5 illustrate evidence of a distinct E-W phase (Fig. 2; Years 0 and 1). The lack of a distinct E-W phase in the models physically means that the models also lack the characteristic propagation features of the PDP. Hence, we could argue that these climate models simulate a North Pacific process very different from how we define and how we view the PDP in nature. ACCESS-CM2 and CESM2-WACCM include evidence for some precession, shown by slight cyclonic rotation of the anomaly dipole with time, though the magnitude of the anomaly dipole for the E-W phase is much less than in reanalysis (Fig. 2, top row). Several other models (e.g.,UKESM1-0-LL and BCC-ESM1) instead show evidence of a damping of the N-S phase of the PDP with time rather than a precession.

To summarize the model results succinctly, we quantitatively compare the models' representation of the N-S phase of the PDP during Year +2, as Year +2 features a distinct N-S phase in reanalysis and the CMIP6 models (Fig. 2, second-to-last column). Aside from the PDP index defined through time-extended EOF analysis, we define an index of the N-S phase of the PDP (i.e., the N-S Index) as the difference in the area-averaged 7-20 year^{-1} band-pass filtered 850 hPa monthly mean geopotential height anomalies between the northern (50°N - 70°N, 175°W - 130°W) and southern (20°N-40°N, 175°W-145°W) loading centers of the N-S phase of the PDP (Fig. 1e, black boxes). This index is essentially the 7-20 year^{-1} bandpass filtered NPO index defined in Furtado et al (2012) with some slight differences in the spatial domain. This formulation also follows from previous work on the PDP and our guiding hypotheses. In addition to the temporal variability of the N-S index, we also calculate the spatial correlation of the structure of the N-S phase of the PDP between the models and reanalysis as a performance metric. Figure 3 summarizes the model performance for the N-S phase of the PDP in a Taylor diagram. Most models under-simulate the observed variability in the N-S phase of the PDP, especially CESM2-WACCM. The difference in variability may result because of a difference in location of the nodes of the N-S phase within model simulations, as noted earlier in Fig. 2. Indeed, excluding CESM2, no model features a N-S phase of the PDP with a pattern correlation with that of the 20th Century

Reanalysis map greater than $r = 0.7$, with most pattern correlations between 0.4 and 0.6 (Fig. 3). Hence, in addition to the differences in their spatial representation of the PDP, these quantification metrics from the Taylor diagram indicate that the CMIP6 models poorly represent the PDP and its individual phases.

To investigate reasons for the mixed performance of these models in simulating aspects of the PDP, we choose a reduced subset of the CMIP6 models to analyze further in this manuscript. We use Figs. 2 and 3 to guide the choices of these models. As such, the remainder of this manuscript focuses on analyses and diagnostics using three of the "most successful" models in reproducing the PDP (i.e., CESM2, ACCESS-CM2, and UKESM1-0-LL) and two of the "least successful" models (i.e., CanESM5 and BCC-CSM2-MR). Results for the other CMIP6 models shown in Fig. 2 are relegated to Supplemental Material for the reader to examine and will be referenced as needed in later comparisons and analyses.

3.2 Investigating mechanistic links between the PDP and central tropical Pacific SSTa variability

Recall that the N-S phase of the PDP maps onto the NPO. Previous literature has shown evidence that the N-S phase of the PDP is linked to fluctuations in central tropical Pacific SST variability and the CP ENSO phenomenon, particularly at quasi-decadal timescales (Di Lorenzo et al, 2010; Furtado et al, 2012). Furthermore, Anderson et al (2016) hypothesized that the warming and cooling patterns in the central tropical Pacific may dynamically drive the N-S phase of the PDP via atmospheric and oceanic pathways. We now investigate this hypothesis directly by comparing the concomitant SSTa evolution in the central tropical Pacific during the emergence of the N-S phase of the PDP and boreal wintertime variability of central tropical Pacific SSTa in both reanalysis and our subset of the CMIP6 models.

Reanalysis supports the hypothesis tying tropical Pacific SSTa variability to the N-S phase of the PDP. Figure 4 shows the lag regression of NDJFM-averaged SSTa in the tropical Pacific from HadISST onto the observed PDP index. Anomalously positive central tropical Pacific SSTa occur with the transition of the PDP from the E-W phase to its N-S orientation (Fig. 4d-f), suggesting a potential lagged relationship between tropical Pacific SSTa and the N-S phase of the PDP. More specifically, the Year +1 pattern (i.e., SSTa lagging the PDP index, Fig. 4e) results in a similar broad area of significant positive SSTa throughout the central tropical Pacific, with negative SSTa in the western Pacific. This is one year prior to the establishment of the N-S phase of the PDP at Year +2. Interestingly, the SSTa patterns at Year 0 and Year +1 suggest that most of the eastern tropical Pacific experiences warming in addition to the central Pacific, characteristic of canonical ENSO conditions. While Anderson et al (2017) hypothesized that the SSTa pattern associated with the emergence of the N-S phase of the PDP is related to CP ENSO variability, the pattern shown in Fig. 4e suggests that the PDP-related SSTa pattern resembles more the decadal expression of ENSO instead (e.g., Zhang et al, 1997; Gu and Philander, 1997; An and Wang, 2000; Choi et al, 2013). We next focus on the SSTa pattern at Year +2 which occurs simultaneously with the N-S phase of the PDP.

Transitioning to analyzing the CMIP6 models, Figure 5 shows the regression of model simulated SSTa onto the PDP index at Year +2 (i.e., the PDP leads SSTa). The resulting SSTa regression patterns show little consistency with reanalysis (Fig 5a), with only BCC-ESM1 (Supplementary Figure S1a) and GISS-E2-1-H (Supplementary Fig. S1d) reproducing the significant relationship between warm central Pacific SSTa and the N-S phase of the PDP. The lack of statistically significant SSTa in most models (Figs. 5b-e) suggests that the large inter-model diversity is likely due to either a lack of ocean-atmosphere dynamics or other physical processes being simulated in CMIP6 models or erroneous temporal variability in tropical Pacific SSTa. Interestingly, both BCC-CSM2-MR (Fig. 5e) and CESM2 (Fig. 5b) show statistically significant ($p < 0.05$) *negative* SSTa in the tropical Pacific, which is dynamically inconsistent with the North Pacific atmospheric response (e.g., Di Lorenzo et al, 2010; Furtado et al, 2012). Models such as BCC-CSM2-MR (Fig. 5e) and CESM2 (Fig. 5b) with statistically significant negative SSTa during Year +2 of the PDP suggest the cause of CMIP6 models lacking a relationship between the PDP and SSTa in the central tropical Pacific may not be just temporal in nature (e.g., Deser et al, 2012),but physical as well. Therefore, the CMIP6 models studied here do not support the working hypothesis on the connections between the tropical Pacific and the N-S phase of the PDP. These results hold consistent for the regression of model simulated SSTa onto the PDP index at Year +1 as well (not shown), indicating that models do not capture even the strongest SSTa signal associated with the transition of the PDP to the N-S phase.

Our next analysis is motivated by the similarities between the CP ENSO spatial pattern from Ashok et al (2007), the regression results from observations in Fig. 5, and prior knowledge that some "flavors" of ENSO are decadal in nature lead us to next investigate whether low-frequency variance in either canonical ENSO or CP ENSO events are associated with the transition to the N-S phase of the PDP from Year +1 to Year +2. With the motivation that the lack of statistical connection between the PDP and central tropical Pacific SSTa (Fig. 5b-e) may be a result of models poorly simulating general Pacific climate variability, figures 6 and 7 illustrate the resulting canonical (Fig. 6) and CP ENSO (Fig. 7) patterns from HadISST and the five CMIP6 models. The results from HadISST are as expected: (1) For canonical ENSO (Fig. 6a), the location of maximum variability is confined to the eastern Pacific; and (2) the location of the maximum anomalies for CP ENSO is located in the central Pacific. Moreover, the CP ENSO structure (Fig. 7a) shows SSTa variability extending toward the coast of southwestern North America, similar to the structure of the SSTa pattern at Years +1 and +2 (Figs. 4e-f). The better match between the CP ENSO structure and the PDP Year +2 SSTa pattern is also confirmed temporally at low frequencies. That is, the correlation between the low-pass filtered (7-20 yr^{-1}) time series of the PDP Year +2 SSTa pattern and that of the canonical ENSO structure in reanalysis is weak ($r = 0.13$). However, the same time series correlated with the filtered CP ENSO time series has a significantly high correlation ($r = 0.85$; $p \ll 0.001$). This high correlation value thus bolsters Hypothesis #1 of our work.

The CMIP6 model simulations, however, show considerable differences in the structures of the two types of ENSO events. For example, the ACCESS-CM2 (Fig. 6c) and BCC-CSM2-MR (Fig. 6e) models have much more variability in SSTa associated with canonical ENSO events than observed. Additionally, with the ex-

ception of CESM2 (Fig. 6b), the CMIP6 models exhibit maximum SSTa variability associated with canonical ENSO events focused on a narrow belt along the cold tongue region instead of the broader meridional structure seen in observations (Fig. 6a). The narrow belt of variability likely influences the models' representation of CP ENSO events, as most models display a CP ENSO structure with maximum SSTa variability eastward of the location shown in reanalysis (Fig. 7) that is more reminiscent of canonical ENSO events. CESM2 (Fig. 7b) is again an exception to this result, with maximum positive SSTa farther west than in reanalysis. Should the N-S phase of the PDP be dynamically linked to CP ENSO conditions, the lack of proper spatial structure and variability for CP ENSO in CMIP6 models supports our earlier findings of CMIP6 model's mixed fidelity of simulations of the N-S phase of the PDP (Fig. 3) and the lack of significant correlation between the two (Fig. 5). Despite these important differences, notice that the pattern correlations between the models and the observed ENSO structures are fairly high in many cases ($r \approx 0.7 - 0.9$ for canonical ENSO (Fig. 6) and $r = 0.8 - 0.9$ for CP ENSO (Fig. 7)). The apparent difference in the quantitative vs. qualitative measures of success indicate the importance for both when considering model performance for the different ENSO flavors. Similar mixed performance exists for the other CMIP6 models with their canonical and CP ENSO structures (Supplemental Figures S2 and S3). GISS-E2-1-G and GISS-E2-1-H show a canonical ENSO structure closely matching HadISST (pattern correlations of $r \sim 0.8 - 0.9$; Supplemental Figs. S2c and S2d), while MIROC6 displays a basin-wide structure (Supplemental Fig. S2f). The CP ENSO structure in these additional models are also too strong in magnitude and, despite high pattern correlations, also erroneously extend throughout the equatorial Pacific (Supplemental Fig. S3). Hence, we conclude that, collectively, these CMIP6 models continue to exhibit known biases in their structure of ENSO flavors (Bellenger et al, 2014).

With biases in the structures of CP ENSO quantified above, we next turn to understanding the temporal variability of CP ENSO structures in reanalysis and the CMIP6 models. This analysis is important because the PDP itself possesses quasi-decadal periodicity (about 12 years), and the guiding hypothesis links this variability in large part to tropical Pacific decadal variability. Thus, not only are the spatial characteristics of the remote forcing important but the timescale of the remote forcing as well. Figure 8 compares the power spectra of the CP ENSO index (i.e., the principal component time series from the EOF analysis) in reanalysis and the five CMIP6 models. As also shown by Furtado et al (2012), the observed CP ENSO phenomenon has significant ($p < 0.05$; red line in all panels of Fig. 8) power on quasi-decadal time scales (Fig. 8a). The selected models, by contrast, generally show power for their respective CP ENSO patterns at higher frequencies than found in reanalysis. For example, ACCESS-CM2 (Fig. 8c) has a statistically significant peak at ∼2-3 years and CESM2 (Fig. 8b) has a statistically significant peak at ∼5 years. Both CESM2 and UKESM1-0-LL (Fig. 8b and f) have significant peaks at quasi-decadal frequencies, yet they are not as robust nor as broad as the peak shown in reanalysis (Fig. 8a). Other CMIP6 models feature similar higher-than-observed frequencies for the CP ENSO phenomenon in their simulations (Supplemental Figure S4). Power spectral analysis conducted on canonical ENSO indices for each model shows no significant quasi-decadal peaks either (Supplemental Figure S5), indicating that the simulated PDP patterns are also not tied temporally to canonical ENSO variability in the models. Overall,

these power spectra further support the idea that the models cannot adequately represent the spatio-temporal evolution of central tropical Pacific SSTa variability, hence likely biasing their representation of the N-S phase of the PDP.

Our final comparison explicitly examines the PDP-related tropical Pacific SSTa pattern (Fig. 4e) in reanalysis and the models. This analysis complements our previous look at canonical and CP ENSO variability but relies on the actual SSTa forcing pattern identified for reanalysis rather than an EOF-defined pattern. To do this analysis, we construct a time series of the PDP-related SSTa pattern by taking the difference of the spatially-averaging SSTa in the two boxes shown in the figure: the central tropical Pacific (10°S - 10°N, 175°W - 130°W) and the western Pacific (0° - 20°N, 135°E - 150°E). These regions were selected due to their statistically significant relationship to the PDP during Year 0, Year +1, and the similar SSTa pattern in Year +2 (Fig. 4). We then apply a 7-20yr^{-1} band-pass filter to the time series and lag-correlate it with the PDP index. Figure 9 shows the lag correlation between the filtered PDP-related SSTa time series and the PDP index. In reanalysis (Fig. 9a), statistically significant ($p < 0.05$) correlations between the two indices at lags Year 0, Year +1, and Year +2. Further, significant negative correlations at lags Year -5 and Year -4 correspond to the evolution of cooler central Pacific SSTa associated with the opposite polarity of the N-S phase of the PDP. By contrast, models show little evidence of any lagged relationship between CP ENSO and the PDP index, with few models having $r > 0.2$ and no apparent periodicity in the lag correlations. The lack of periodicity matches the models' absence of significant precession associated with the PDP (Fig.2). In fact, the ACCESS-CM2 (Fig. 9c) shows a statistically significant correlation at Years -5 and -4, however the correlation is positive which is not consistent with reanalysis (i.e., should be negative / related to negative SSTa). The other CMIP6 models also have poor representation of the lag correlations between their PDP-related SSTa pattern and PDP index (Supplemental Figure S6). Overall, these results further highlight how models struggle to simulate the relationship between the PDP and tropical Pacific SSTa variability as seen in reanalysis (Fig. 9).

3.3 Evaluating teleconnections between the PDP and the tropical Pacific

The last section addresses Hypothesis #2 – i.e., examining tropical Pacific-extratropical North Pacific teleconnection pathways associated with the PDP. The proposed mechanism asserts an "atmospheric bridge" mechanism linking the PDP and the tropics. That is, variations in the longitudinal location of diabatic heating in the tropics can induce different Rossby wave patterns which subsequently modulate atmospheric circulation in the extratropics (Hoskins and Karoly, 1981; Alexander et al, 2002). We investigate the proposed atmospheric bridge mechanism for the PDP in both reanalysis and models using our index of the PDP-related SSTa pattern (Section 3.2 and Fig. 5a). Supplementary Figure S7 affirms that this method captures the desired forcing pattern in the models and reanalysis, with pattern correlations between model results and reanalysis ranging from $r = 0.88$ for BCC-CSM2-MR (Supplementary Fig. S7e) to $r = 0.95$ for HadGEM3-GC31-LL (Supplementary Fig. S7k). While the pattern correlations are high, slight variation in the location of maximum positive SSTa is apparent, with some models simulating it farther west (CESM2, CESM2-WACCM) and some simulating it farther east

(GISS-E2-1-G, HadGEM3-GC31-LL). Model biases in the climatological state of the tropical Pacific may play a role in the variability of these patterns across different models and will need to be investigated.

Next, Figure 10 presents the regression of 7-20 year^{-1} band-pass filtered 500 hPa eddy (i.e., zonal-mean removed) geopotential height anomalies onto the bandpass-filtered PDP-related SST index. In reanalysis (Fig. 10a), the N-S phase of the PDP emerges in the North Pacific as expected, with opposite-signed anomalies over East Asia and anomalous troughing downstream across eastern North America. These reanalysis results are consistent with those found in Furtado et al (2012); namely, that low-frequency variability in the central tropical Pacific SST forces a north-south oriented dipole in geopotential height anomalies in the North Pacific. By contrast, the results from CMIP6 model output vary considerably in their atmospheric responses to these similar SSTa changes in the central and western tropical Pacific (Figs. 10b-f). Overall, model teleconnection patterns appear to map more onto the Pacific-North American (PNA) pattern (Horel and Wallace, 1981; Wallace and Gutzler, 1981) as opposed to the N-S phase of the PDP/the NPO. Intensification of the Aleutian Low appears in every model, which is actually the preferred atmospheric response to canonical ENSO episodes, not CP ENSO events or quasi-decadal tropical Pacific forcing (e.g., Alexander et al, 2002; Di Lorenzo et al, 2010; Furtado et al, 2012; Di Lorenzo et al, 2015). Moreover, the spatial correlation of the 500 hPa eddy geopotential height anomaly maps in the North Pacific between any model and reanalysis does not exceed $r = 0.6$. The large biases in the simulated wave trains for model output with respect to reanalysis suggest that the atmospheric dynamics in models are not representative of those in observations on the quasi-decadal time scale. The other CMIP6 models also feature the same biases (Supplemental Figure S8). Interestingly, the CMIP6 models struggle with similar biases to models used in the Intergovernmental Panel on Climate Change (IPCC) Fourth Assessment Report (AR4) (Furtado et al, 2011). Since we know that central tropical Pacific SSTa variability forces an NPO-like response at high and low frequencies (Furtado et al, 2012), these documented biases in the CMIP6 models point to model deficiencies in their ENSO structures and frequencies (Figs. 6-9) and/or potentially incorrectly capturing the atmospheric bridge mechanism associated with tropical and extratropical Pacific teleconnections

4 Summary & Discussion

This study expanded our knowledge on a newly-identified model of Pacific decadal climate variability – the PDP – through testing leading hypotheses on its dynamical mechanisms in both reanalysis and a subset of the latest climate models in the CMIP6 model archive. Our results demonstrated a relationship between the N-S phase of the PDP (related to the NPO) and central tropical Pacific climate variability. Several key analyses established this relationship. The SSTa pattern associated with the emergence of the N-S phase of the PDP (i.e., the PDP Year 0,+1 and +2 SSTa pattern) is similar the structure of CP ENSO in HadISST (Fig. 4). The CP ENSO time series derived for HadISST had significant power at quasi-decadal frequencies (Fig. 8), was highly correlated with the time series of the PDP-related SSTa pattern ($r = 0.85, p \ll 0.001$), and is significantly correlated with the PDP index at lag Year +1 (Fig. 9a). We performed the same analysis

with canonical ENSO indices, and no significant relationship was found between those indices and the N-S phase of the PDP pattern ($r \approx 0.13$; not shown). This lack of a relationship makes sense statistically since the canonical ENSO structure is nearly orthogonal to the CP ENSO structure, which *is* related to the N-S phase of the PDP, and has little power at quasi-decadal frequencies but maximizes in interannual frequencies (Supplementary Fig. S4). Based on these results, low frequency variations in CP ENSO are indeed strongly related to the N-S phase of the PDP.

When examining the PDP and its dynamical mechanisms within the CMIP6 models, we find that the models feature strong biases in several facets of the PDP. First, the models erroneously simulate both the spatial signature and magnitude of the PDP, especially the E-W phase (Fig. 2). Second, simulations of the PDP's relationship to central tropical Pacific SSTa at lag Year +2 in CMIP6 models is weak, with few showing statistically significant anomalies in the same region as in reanalysis and some showing anomalies of the wrong sign (Figs. 4 and 5). Our findings with the CMIP6 models mirror those of Anderson et al (2017), who examined how the PDP was represented in the Community Climate System Model version 4 (CCSM4; Gent et al, 2011). Their results indicated that the CCSM4 simulates the PDP as a stationary damping and periodic flipping of the N-S phase and does *not* capture the concomitant evolution of central tropical Pacific SSTa. Moreover, parallel statistical analyses with the model output (e.g., the power spectra of CP ENSO, lag regressions with Pacific SSTa) indicate continued misrepresentations of the secondary mode paradigm for the North Pacific (i.e., the CP ENSO and NPO; Figs. 8 and 9). Since the N-S phase of the PDP is influenced by CP ENSO, then the inability of models in capturing the connection between the central tropical Pacific and the North Pacific introduces errors into their simulations of the PDP. Therefore, biases in tropical and North Pacific decadal climate variability remain a problem for these climate models even in their newest generation and need to be corrected for improved climate projections (e.g., Furtado et al, 2011; Bellenger et al, 2014; Yim et al, 2015; Liu and Di Lorenzo, 2018; Zhao et al, 2020). While not explicitly studied in this manuscript, the problems leading to these mismatches in spatio-temporal variability of the Pacific decadal climate modes likely arises from wrong ocean-atmosphere coupling dynamics, including those associated with the meridional modes (e.g., Chiang and Vimont, 2004; Di Lorenzo et al, 2015; You and Furtado, 2018; Liu and Di Lorenzo, 2018). Should CP ENSO events increase in frequency and/or magnitude, as is expected under anthropogenic climate change (Yeh et al, 2009; Freund et al, 2019), then the resulting Pacific climate regimes may be very different than those projected by the models. Hence, these likely changes in the projected future Pacific climate regimes are further motivation to make sure we understand modes like the PDP and learn to understand what elements of ENSO diversity and tropical-extratropical atmospheric (and oceanic) pathways need to be corrected in the models.

Synthesizing the relationship between the PDP and the NPO in reanalysis, including its links to the central tropical Pacific, results in a robust argument to include the PDP within the secondary mode paradigm for Pacific variability. Yet, the CMIP6 models do not support this conclusion. Therefore how the PDP is placed within this paradigm requires further research. For example, relationships between the PDP and other climate modes in the Pacific, including the Madden-Julian Osciallation, variability in the Kuroshio-Oyoshio Current (Anderson, 2019),

and the meridional modes, need to be quantified. One particular link to the PDP yet to be explored is the connections between the PDP and the NPGO. The secondary mode paradigm establishes that the NPO forces variability in the NPGO (Chhak et al, 2009; Furtado et al, 2011; Di Lorenzo et al, 2015). With our results showing that the N-S phase of the PDP maps onto the NPO and the concomitant SSTa evolution in the tropics related to CP ENSO, which is a forcing for the NPO (Furtado et al, 2012), there is likely a link between the PDP and the NPGO on the quasi-decadal timescale. Furthermore, SSTa in the North Pacific can substantially impact the overlying circulation (Frankignoul and Sennéchael, 2007), so the underlying North Pacific SSTa field may influence the evolution of the PDP as well (Anderson, 2019).

While this work investigated the evolution and dynamics associated with the N-S phase of the PDP, we have not addressed the other phase of the PDP - i.e., the E-W phase. This phase is particularly interesting for two reasons. First, the E-W phase of the PDP may be connected more with extratropical forcing, including that from the polar stratosphere, than tropical Pacific SSTa variability, at least indirectly (Anderson et al, 2017). Indeed, Domeisen et al (2019) found that the state of the polar stratospheric vortex is profoundly affected by ENSO variability, with more sudden stratospheric warmings (SSWs; i.e., a rapid weakening of the stratospheric polar vortex) occurring during El Niño years. SSWs can have a strong impact on the underlying tropospheric circulation (Baldwin and Dunkerton, 1999; Baldwin et al, 2001) and may have decadal variability (van Loon and Labitzke, 2011; Hu and Guan, 2018). The second reason is that the models which perform poorly at simulating the PDP do so because they lack a transition from the N-S phase to the E-W phase (Fig. 2). AOGCMs poorly simulate stratosphere-troposphere coupling dynamics in the tropics and extratropics (e.g., Charlton-Perez et al, 2013; Furtado et al, 2015; Seviour et al, 2016). Even models with high tops (i.e., model tops generally above 10 hPa) like CESM2-WACCM show no noticeable improvement in their simulation of the E-W phase within this study. Should the E-W phase of the PDP be forced in part by the stratosphere, further improvement of stratospheric resolution and dynamics will be important in improving predictions of this mode of variability. In fact, the E-W phase of the PDP strongly affects decadal variability in seasonal precipitation in the Northwestern US and the Great Plains (Anderson et al, 2016). Thus, understanding and capturing the E-W phase of the PDP may have profound impacts on long-lead extreme precipitation events across the western US and improved projections of hydroclimate extremes under future climate change.

Acknowledgements 20th Century Reanalysis V2c data provided by the NOAA/OAR/ESRL PSL, Boulder, Colorado, USA, from their Web site at `https://psl.noaa.gov/`. Support for the 20th Century Reanalysis Project version 2c dataset is provided by the U.S. Department of Energy, Office of Science Biological and Environmental Research (BER), and by the National Oceanic and Atmospheric Administration Climate Program Office. The authors acknowledge the World Climate Research Programme, which, through its Working Group on Coupled Modelling, coordinated and promoted CMIP6. We thank the climate modeling groups for producing and making available their model output, the Earth System Grid Federation (ESGF) for archiving the data and providing access, and the multiple funding agencies who support CMIP6 and ESGF.

References

Alexander MA, Bladé I, Newman M, Lanzante JR, Lau NC, Scott JD (2002) The atmospheric bridge: The influence of ENSO teleconnections on air–sea interaction over the global oceans. Journal of Climate 15:2205–2231, 10.1175/1520-0442(2002)015⟨2205:TABTIO⟩2.0.CO;2

An SI, Wang B (2000) Interdecadal change of the structure of the ENSO mode and its impact on the ENSO frequency. Journal of Climate 13:2044–2055, 10.1175/1520-0442(2000)013⟨2044:ICOTSO⟩2.0.CO;2

Anderson BT (2019) Empirical evidence linking the Pacific Decadal Precession to Kuroshio Extension variability. Journal of Geophysical Research: Atmospheres 124:12,845–12,863, 10.1029/2019JD031163

Anderson BT, Gianotti DJS, Furtado JC, Di Lorenzo E (2016) A decadal precession of atmospheric pressures over the North Pacific. Geophysical Research Letters 43:3921–3927, 10.1002/2016GL068206

Anderson JC Bruce Tand Furtado, Di Lorenzo E, Short Gianotti DJ (2017) Tracking the Pacific Decadal Precession. Journal of Geophysical Research 122:3214–3227, 10.1002/2016JD025962

Ashok K, Behera SK, Rao SA, Weng H, Yamagata T (2007) El Niño Modoki and its possible teleconnection. Journal of Geophysical Research: Oceans 112:1–27, 10.1029/2006JC003798

Baldwin MP, Dunkerton TJ (1999) Propagation of the Arctic Oscillation from the stratosphere to the troposphere. Journal of Geophysical Research Atmospheres 104(D24):30,937–30,946, 10.1029/1999JD900445

Baldwin MP, Gray LJ, Dunkerton TJ, Hamilton K, Haynes PH, Randel WJ, Holton JR, Alexander MJ, Hirota I, Horinouchi T, Jones DBA, Kinnersley JS, Marquardt C, Sato K, Takahashi M (2001) The Quasi-Biennial Oscillation. Reviews of Geophysics 39:179–229, 10.1029/1999RG000073

Baxter S, Nigam S (2015) Key role of the North Pacific Oscillation–West Pacific pattern in generating the extreme 2013/14 North American winter. Journal of Climate 28:8109–8117, 10.1175/JCLI-D-14-00726.1

Bellenger H, Guilyardi E, Leloup J, Lengaigne M, Vialard J (2014) ENSO representation in climate models: From CMIP3 to CMIP5. Climate Dynamics 42:1999–2018, 10.1007/s00382-013-1783-z

Bond NA, Cronin MF, Freeland H, Mantua N (2015) Causes and impacts of the 2014 warm anomaly in the NE Pacific. Geophysical Research Letters 42:3414–3420, 10.1002/2015GL063306

Capotondi A, Sardeshmukh PD, Ricciardulli L (2018) The nature of the stochastic wind forcing of ENSO. Journal of Climate 31:8081–8099, 10.1175/JCLI-D-17-0842.1

Charlton-Perez AJ, Baldwin MP, Birner T, Black RX, Butler AH, Calvo N, Davis NA, Gerber EP, Gillett N, Hardiman S, Kim J, Krüger K, Lee YY, Manzini E, McDaniel BA, Polvani L, Reichler T, Shaw TA, Sigmond M, Son SW, Toohey M, Wilcox L, Yoden S, Christiansen B, Lott F, Shindell D, Yukimoto S, Watanabe S (2013) On the lack of stratospheric dynamical variability in low-top versions of the CMIP5 models. Journal of Geophysical Research: Atmospheres 118:2494–2505, 10.1002/jgrd.50125

Cheung WW, Frölicher TL (2020) Marine heatwaves exacerbate climate change impacts for fisheries in the northeast Pacific. Scientific Reports 10:1–10, 10.1038/

s41598-020-63650-z
Chhak KC, Di Lorenzo E, Schneider N, Cummins PF, Chhak KC, Lorenzo ED, Schneider N, Cummins PF (2009) Forcing of low-frequency ocean variability in the Northeast Pacific. Journal of Climate 22:1255–1276, 10.1175/2008JCLI2639.1
Chiang JC, Vimont DJ (2004) Analogous Pacific and Atlantic Meridional Modes of tropical atmosphere-ocean variability. Journal of Climate 17:4143–4158, 10.1175/JCLI4953.1
Choi J, An Prof SI, Yeh SW, Yu JY (2013) ENSO-like and ENSO-induced tropical pacific decadal variability in CGCMs. Journal of Climate 26:1485–1501, 10.1175/JCLI-D-12-00118.1
Compo GP, Whitaker JS, Sardeshmukh PD, Matsui N, Allan RJ, Yin X, Gleason BE, Vose RS, Rutledge G, Bessemoulin P, Brönnimann S, Brunet M, Crouthamel RI, Grant AN, Groisman PY, Jones PD, Kruk MC, Kruger AC, Marshall GJ, Maugeri M, Mok HY, Nordli Ø, Ross TF, Trigo RM, Wang XL, Woodruff SD, Worley SJ (2011) The Twentieth Century Reanalysis Project. Quarterly Journal of the Royal Meteorological Society 137:1–28, 10.1002/qj.776
Cook BI, Williams AP, Mankin JS, Seager R, Smerdon JE, Singh D (2018) Revisiting the leading drivers of Pacific coastal drought variability in the contiguous United States. Journal of Climate 31:25–43, 10.1175/JCLI-D-17-0172.1
Cox CJ, Stone RS, Douglas DC, Stanitski DM, Gallagher MR (2019) The Aleutian Low-Beaufort Sea anticyclone: A climate index correlated with the timing of springtime melt in the Pacific Arctic cryosphere. Geophysical Research Letters 46:7464–7473, 10.1029/2019GL083306
Danabasoglu G (2019) NCAR CESM2-WACCM model output prepared for CMIP6 CMIP piControl. 10.22033/ESGF/CMIP6.10094
Danabasoglu G, Lawrence D, Lindsay K, Lipscomb W, Strand G (2019) NCAR CESM2 model output prepared for CMIP6 CMIP piControl. 10.22033/ESGF/CMIP6.7733
Deser C, Phillips AS, Tomas RA, Okumura YM, Alexander MA, Capotondi A, Scott JD, Kwon YO, Ohba M (2012) ENSO and Pacific decadal variability in the Community Climate System Model Version 4. Journal of Climate 25:2622–2651, 10.1175/JCLI-D-11-00301.1
Deser C, Simpson IR, McKinnon KA, Phillips AS (2017) The Northern Hemisphere extratropical atmospheric circulation response to ENSO: How well do we know it and how do we evaluate models accordingly? Journal of Climate 30:5059–5082, 10.1175/JCLI-D-16-0844.1
Di Lorenzo E, Mantua N (2016) Multi-year persistence of the 2014/15 North Pacific marine heatwave. Nature Climate Change 6:1042–1047, 10.1038/nclimate3082
Di Lorenzo E, Schneider N, Cobb KM, Franks PJS, Chhak K, Miller AJ, McWilliams JC, Bograd SJ, Arango H, Curchitser E, Powell TM, Rivière P (2008) North Pacific Gyre Oscillation links ocean climate and ecosystem change. Geophysical Research Letters 35:L08,607, 10.1029/2007GL032838
Di Lorenzo E, Cobb KM, Furtado JC, Schneider N, Anderson BT, Bracco A, Alexander MA, Vimont DJ (2010) Central Pacific El Niño and decadal climate change in the North Pacific Ocean. Nature Geoscience 3:762–765, 10.1038/ngeo984

718 Di Lorenzo E, Liguori G, Schneider N, Furtado JC, Anderson BT, Alexander
719 MA (2015) ENSO and meridional modes: A null hypothesis for Pacific climate
720 variability. Geophysical Research Letters 42:9440–9448, 10.1002/2015GL066281
721 Diaz HF, Hoerling MP, Eischeid JK (2001) ENSO variability, teleconnections and
722 climate change. International Journal of Climatology 21:1845–1862, 10.1002/
723 joc.631
724 Diffenbaugh NS, Swain DL, Touma D (2015) Anthropogenic warming has increased
725 drought risk in California. Proceedings of the National Academy of Sciences
726 112:3931–3936, 10.1073/pnas.1422385112
727 Dix M, Bi D, Dobrohotoff P, Fiedler R, Harman I, Law R, Mackallah C, Mars-
728 land S, O'Farrell S, Rashid H, Srbinovsky J, Sullivan A, Trenham C, Vohralik
729 P, Watterson I, Williams G, Woodhouse M, Bodman R, Dias FB, Domingues
730 C, Hannah N, Heerdegen A, Savita A, Wales S, Allen C, Druken K, Evans
731 B, Richards C, Ridzwan SM, Roberts D, Smillie J, Snow K, Ward M, Yang
732 R (2019) CSIRO-ARCCSS ACCESS-CM2 model output prepared for CMIP6
733 CMIP piControl. 10.22033/ESGF/CMIP6.4311
734 Domeisen DI, Garfinkel CI, Butler AH (2019) The teleconnection of El Niño South-
735 ern Oscillation to the stratosphere. Review of Geophysics 57:5–47, 10.1029/
736 2018RG000596
737 Duffy PA, Walsh JE, Graham JM, Mann DH, Rupp TS (2005) Impacts of large-
738 scale atmospheric–ocean variability on Alaskan fire season severity. Ecological
739 Applications 15:1317–1330, 10.1890/04-0739
740 Eyring V, Bony S, Meehl GA, Senior CA, Stevens B, Stouffer RJ, Taylor KE (2016)
741 Overview of the Coupled Model Intercomparison Project Phase 6 (CMIP6) ex-
742 perimental design and organization. Geoscientific Model Development 9:1937–
743 1958, 10.5194/gmd-9-1937-2016
744 Frankignoul C, Sennéchael N (2007) Observed influence of North Pacific SST
745 anomalies on the atmospheric circulation. Journal of Climate 20:592–606,
746 10.1175/JCLI4021.1
747 Freund MB, Henley BJ, Karoly DJ, McGregor HV, Abram NJ, Dommenget D
748 (2019) Higher frequency of Central Pacific El Niño events in recent decades
749 relative to past centuries. Nature Geoscience 12:450–455, 10.1038/s41561-019
750 -0353-3
751 Furtado JC, Di Lorenzo E, Schneider N, Bond NA (2011) North Pacific decadal
752 variability and climate change in the IPCC AR4 Models. Journal of Climate
753 24:3049–3067, 10.1175/2010JCLI3584.1
754 Furtado JC, Di Lorenzo E, Anderson BT, Schneider N (2012) Linkages between the
755 North Pacific Oscillation and central tropical Pacific SSTs at low frequencies.
756 Climate Dynamics 39:2833–2846, 10.1007/s00382-011-1245-4
757 Furtado JC, Cohen JL, ansd E E Riddle AHB, Kumar A (2015) Eurasian snow
758 cover variability and links to winter climate in the CMIP5 models. Climate Dyn
759 45:2591–2605, https://doi.org/10.1007/s00382-015-2494-4
760 Gent PR, Danabasoglu G, Donner LJ, Holland MM, Hunke EC, Jayne SR,
761 Lawrence DM, Neale RB, Rasch PJ, Vertenstein M, Worley PH, Yang ZL, Zhang
762 M (2011) The Community Climate System Model Version 4. Journal of Climate
763 24:4973–4991, 10.1175/2011JCLI4083.1
764 Goddard L, Dilley M (2005) El Niño: Catastrophe or opportunity. Journal of
765 Climate 18:651–665, 10.1175/JCLI-3277.1

766 Gu D, Philander SGH (1997) Interdecadal Climate Fluctuations That Depend on
767 Exchanges Between the Tropics and Extratropics. Science 275(5301)
768 Hartmann DL (2015) Pacific sea surface temperature and the winter of 2014.
769 Geophysical Research Letters 42(6):1894–1902, 10.1002/2015GL063083
770 Horel JD, Wallace JM (1981) Planetary-scale atmospheric phenomena associated
771 with the Southern Oscillation. Monthly Weather Review 109(4):813–829, 10
772 .1175/1520-0493(1981)109⟨0813:PSAPAW⟩2.0.CO;2
773 Hoskins BJ, Karoly DJ (1981) The steady linear response of a spherical atmo-
774 sphere to thermal and orographic forcing. Journal of the Atmospheric Sciences
775 38(6):1179–1196, 10.1175/1520-0469(1981)038⟨1179:TSLROA⟩2.0.CO;2
776 Hu D, Guan Z (2018) Decadal relationship between the stratospheric Arctic vortex
777 and Pacific Decadal Oscillation. Journal of Climate 31:3371–3386, 10.1175/JCLI
778 -D-17-0266.1
779 Jacox MG, Alexander MA, Siedlecki S, Chen K, Kwon YO, Brodie S, Ortiz I,
780 Tommasi D, Widlansky MJ, Barrie D, Capotondi A, Cheng W, Di Lorenzo E,
781 Edwards C, Fiechter J, Fratantoni P, Hazen EL, Hermann AJ, Kumar A, Miller
782 AJ, Pirhalla D, Pozo Buil M, Ray S, Sheridan SC, Subramanian A, Thompson
783 P, Thorne L, Annamalai H, Aydin K, Bograd SJ, Griffis RB, Kearney K, Kim
784 H, Mariotti A, Merrifield M, Rykaczewski R (2020) Seasonal-to-interannual pre-
785 diction of North American coastal marine ecosystems: Forecast methods, mech-
786 anisms of predictability, and priority developments. Progress in Oceanography
787 183, 10.1016/j.pocean.2020.102307
788 Kim ST, Yu JY (2012) The two types of ENSO in CMIP5 models. Geophysical
789 Research Letters 39(11), 10.1029/2012GL052006
790 Kwon YO, Deser C (2007) North pacific decadal variability in the community cli-
791 mate system model version 2. Journal of Climate 20(11):2416 – 2433, 10.1175/
792 JCLI4103.1, URL https://journals.ametsoc.org/view/journals/clim/20/
793 11/jcli4103.1.xml
794 Litzow MA, Hunsicker ME, Bond NA, Burke BJ, Cunningham CJ, Gosselin JL,
795 Norton EL, Ward EJ, Zador SG (2020) The changing physical and ecological
796 meanings of North Pacific Ocean climate indices. Proceedings of the National
797 Academy of Sciences of the United States of America 117:7665–7671, 10.1073/
798 pnas.1921266117
799 Liu Z, Di Lorenzo E (2018) Mechanisms and predictability of Pacific decadal vari-
800 ability. Current Climate Change Reports 4:128–144, 10.1007/s40641-018-0090-5
801 van Loon H, Labitzke K (2011) Interannual variations in the stratosphere of the
802 Northern Hemisphere: A description of some probable influences. Geophysical
803 Monograph Series, American Geophysical Union (AGU), 10.1029/gm075p0111
804 Mantua NJ, Hare SR, Zhang Y, Wallace JM, Francis RC (1997) A Pacific in-
805 terdecadal climate oscillation with impacts on salmon production. Bulletin of
806 the American Meteorological Society 78(6):1069–1079, 10.1175/1520-0477(1997)
807 078⟨1069:APICOW⟩2.0.CO;2
808 Moore GW (2012) Decadal variability and a recent amplification of the summer
809 Beaufort Sea High. Geophysical Research Letters 39, 10.1029/2012GL051570
810 NASA Goddard Institute for Space Studies (NASA/GISS) (2018a) NASA-GISS
811 GISS-E2.1G model output prepared for CMIP6 CMIP piControl. 10.22033/
812 ESGF/CMIP6.7380
813 NASA Goddard Institute for Space Studies (NASA/GISS) (2018b) NASA-GISS
814 GISS-E2.1H model output prepared for CMIP6 CMIP piControl. 10.22033/

ESGF/CMIP6.7381
Newman M, Compo GP, Alexander MA (2003) ENSO-forced variability of the Pacific Decadal Oscillation. Journal of Climate 16(23):3853–3857, 10.1175/1520-0442(2003)016⟨3853:EVOTPD⟩2.0.CO;2
Newman M, Alexander MA, Ault TR, Cobb KM, Deser C, Di Lorenzo E, Mantua NJ, Miller AJ, Minobe S, Nakamura H, Schneider N, Vimont DJ, Phillips AS, Scott JD, Smith CA (2016) The Pacific Decadal Oscillation, revisited. Journal of Climate 29:4399–4427, 10.1175/JCLI-D-15-0508.1
Pierce DW, Barnett TP, Schneider N, Saravanan R, Dommenget D, Latif M (2001) The role of ocean dynamics in producing decadal climate variability in the North Pacific. Climate Dynamics 18(1-2):51–70, 10.1007/s003820100158
Rayner NA, Parker DE, Horton EB, Folland CK, Alexander LV, Rowell DP, Kent EC, Kaplan A (2003) Global analyses of sea surface temperature, sea ice, and night marine air temperature since the late nineteenth century. Journal of Geophysical Research D: Atmospheres 108(14):4407, 10.1029/2002jd002670
Ridley J, Menary M, Kuhlbrodt T, Andrews M, Andrews T (2018) MOHC HadGEM3-GC31-LL model output prepared for CMIP6 CMIP piControl. 10.22033/ESGF/CMIP6.6294
Rogers JC (1981) The North Pacific Oscillation. Journal of Climatology 1(1):39–57, 10.1002/joc.3370010106
Schneider N, Cornuelle BD (2005) The forcing of the Pacific Decadal Oscillation. Journal of Climate 18(21):4355–4373, 10.1175/JCLI3527.1
Seviour WJM, Gray LJ, Mitchell DM (2016) Stratospheric polar vortex splits and displacements in the high-top CMIP5 climate models. Journal of Geophysical Research: Atmospheres 121(4):1400–1413, 10.1002/2015JD024178
Shakun JD, Shaman J (2009) Tropical origins of north and south pacific decadal variability. Geophysical Research Letters 36(19), https://doi.org/10.1029/2009GL040313, URL https://agupubs.onlinelibrary.wiley.com/doi/abs/10.1029/2009GL040313, https://agupubs.onlinelibrary.wiley.com/doi/pdf/10.1029/2009GL040313
Shi J, Fedorov AV, Hu S (2019) North Pacific temperature and precipitation response to El Niño-like equatorial heating: sensitivity to forcing location. Climate Dynamics 53(5-6):2731–2741, 10.1007/s00382-019-04655-x
Sun T, Okumura YM (2019) Role of stochastic atmospheric forcing from the South and North Pacific in tropical Pacific decadal variability. Journal of Climate 32(13):4013–4038, 10.1175/JCLI-D-18-0536.1
Sung MK, Jang HY, Kim BM, Yeh SW, Choi YS, Yoo C (2019) Tropical influence on the North Pacific Oscillation drives winter extremes in North America. Nature Climate Change 9:1–6, 10.1038/s41558-019-0461-5
Swart NC, Cole JNS, Kharin VV, Lazare M, Scinocca JF, Gillett NP, Anstey J, Arora V, Christian JR, Jiao Y, Lee WG, Majaess F, Saenko OA, Seiler C, Seinen C, Shao A, Solheim L, von Salzen K, Yang D, Winter B, Sigmond M (2019) CCCma CanESM5 model output prepared for CMIP6 CMIP piControl. 10.22033/ESGF/CMIP6.3673
Tang Y, Rumbold S, Ellis R, Kelley D, Mulcahy J, Sellar A, Walton J, Jones C (2019) MOHC UKESM1.0-LL model output prepared for CMIP6 CMIP piControl. 10.22033/ESGF/CMIP6.6298
Tatebe H, Watanabe M (2018) MIROC MIROC6 model output prepared for CMIP6 CMIP piControl. 10.22033/ESGF/CMIP6.5711

Wallace JM, Gutzler DS (1981) Teleconnections in the geopotential height field during the Northern Hemisphere winter. Monthly Weather Review 109(4):784–812, 10.1175/1520-0493(1981)109⟨0784:TITGHF⟩2.0.CO;2

Wang C (2018) A review of ENSO theories. National Science Review 5(6):813–825, 10.1093/nsr/nwy104

Wang H, Kumar A, Wang W, Xue Y (2012) Influence of ENSO on Pacific decadal variability: An analysis based on the NCEP Climate Forecast System. Journal of Climate 25(18):6136–6151, 10.1175/JCLI-D-11-00573.1

Wills RC, Battisti DS, Proistosescu C, Thompson LA, Hartmann DL, Armour KC (2019) Ocean circulation signatures of North Pacific decadal variability. Geophysical Research Letters 46(3):1690–1701, 10.1029/2018GL080716

Wu T, Chu M, Dong M, Fang Y, Jie W, Li J, Li W, Liu Q, Shi X, Xin X, Yan J, Zhang F, Zhang J, Zhang L, Zhang Y (2018) BCC BCC-CSM2MR model output prepared for CMIP6 CMIP piControl. 10.22033/ESGF/CMIP6.3016

Yeh SW, Kug JS, Dewitte B, Kwon MH, Kirtman BP, Jin FF (2009) El Niño in a changing climate. Nature 461:511–514, 10.1038/nature08316

Yeh SW, Cai W, Min SK, McPhaden MJ, Dommenget D, Dewitte B, Collins M, Ashok K, An SI, Yim BY, Kug JS (2018) ENSO Atmospheric Teleconnections and Their Response to Greenhouse Gas Forcing. Reviews of Geophysics pp 185–206, https://doi.org/10.1002/2017RG000568

Yim BY, Kwon M, Min SH, Kug JS (2015) Pacific Decadal Oscillation and its relation to the extratropical atmospheric variation in CMIP5. Climate Dynamics 44:1521–1540, 10.1007/s00382-014-2349-4

You Y, Furtado JC (2018) The South Pacific Meridional Mode and its role in tropical Pacific climate variability. Journal of Climate 31:10,141–10,163, 10.1175/JCLI-D-17-0860.1

Zhang C (2005) Madden-Julian Oscillation. Review of Geophysics 43(2):1–36, 10 .1029/2004RG000158

Zhang J, Wu T, Shi X, Zhang F, Li J, Chu M, Liu Q, Yan J, Ma Q, Wei M (2018a) BCC BCC-ESM1 model output prepared for CMIP6 CMIP piControl. 10.22033/ESGF/CMIP6.3017

Zhang Y, Wallace JM, Battisti DS (1997) ENSO-like interdecadal variability: 1900-93. Journal of Climate 10(5):1004–1020, 10.1175/1520-0442(1997)010⟨1004:ELIV⟩2.0.CO;2

Zhang Y, Xie SP, Kosaka Y, Yang JC (2018b) Pacific Decadal Oscillation: Tropical Pacific forcing versus internal variability. Journal of Climate 31(20):8265–8279, 10.1175/JCLI-D-18-0164.1

Zhao Y, Di Lorenzo E, Sun D, Stevenson S (2020) Tropical Pacific decadal variability and ENSO precursor in CMIP5 Models. Journal of Climate p 1, 10.1175/jcli-d-20-0158.1

Model Data			
Model	**Institution ID**	**Label**	**References**
ACCESS-CM2	CSIRO-ARCCSS	Australian Community Climate and Earth System Simulator Climate Model Version 2	Dix et al (2019)
BCC-CSM2-MR	BCC	BCC-CSM 2 MR	Wu et al (2018)
BCC-ESM1	BCC	BCC-ESM1	Zhang et al (2018a)
CanESM5	CCCma	Canadian Earth System Model version 5	Swart et al (2019)
CESM2	NCAR	Community Earth System Model version 2	Danabasoglu et al (2019)
CESM2-WACCM	NCAR	Community Earth System Model version 2 - Whole Atmosphere Community Climate Model	Danabasoglu (2019)
GISS-E2-1-G	NASA-GISS	GISS-E2.1G	NASA Goddard Institute for Space Studies (NASA/GISS) (2018a)
GISS-E2-1-H	NASA-GISS	GISS-E2.1H	NASA Goddard Institute for Space Studies (NASA/GISS) (2018b)
HadGEM3-GC31-LL	MOHC NERC	HadGEM3-GC3.1-N96ORCA1	Ridley et al (2018)
MIROC6	MIROC	MIROC6	Tatebe and Watanabe (2018)
UKESM1-0-LL	MOHC NERC NIMS-KMA NIWA	UKESM1.0-N96ORCA1	Tang et al (2019)

Table 1 Information and references for CMIP6 model output used in this study.

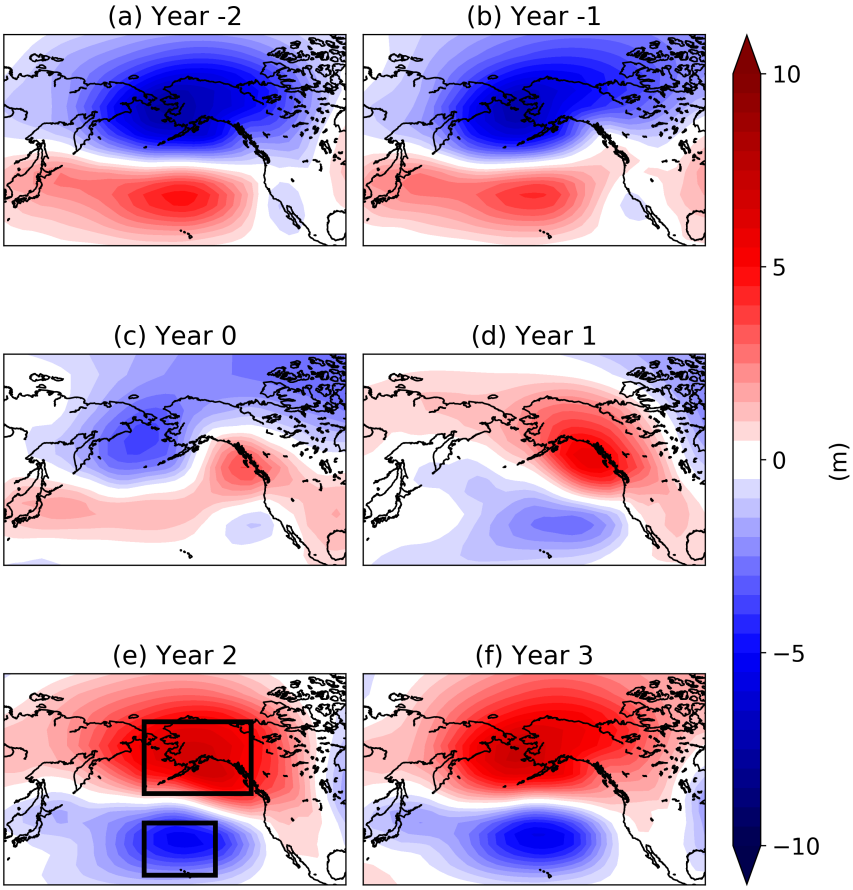

Fig. 1 Regression of 7-20 year^{-1} band-passed 850 hPa November-March (NDJFM) averaged monthly-mean geopotential height anomalies (m) onto the standardized PDP index for lags of Year -2 to Year +3 for the 20th Century Reanalysis version 2c. Positive lags indicate the PDP index leads the geopotential height field and vice versa for negative lags. Black boxes in (e) designate the northern (50°N - 70°N, 175°W - 130°W) and southern (20°N - 40°N, 175°W - 145°W) domains used to define the N-S Index (see text).

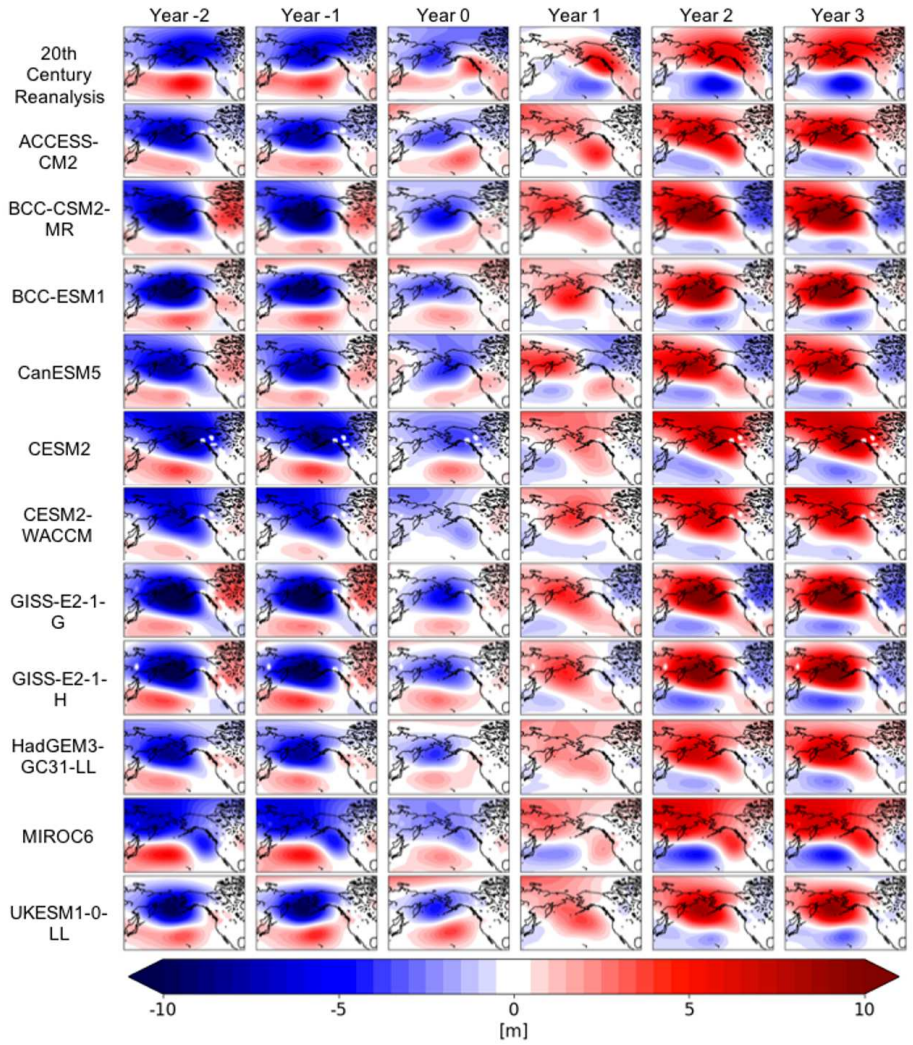

Fig. 2 (first row) Same as Fig. 1. (all other rows) As in Fig. 1 but for the various CMIP6 model output.

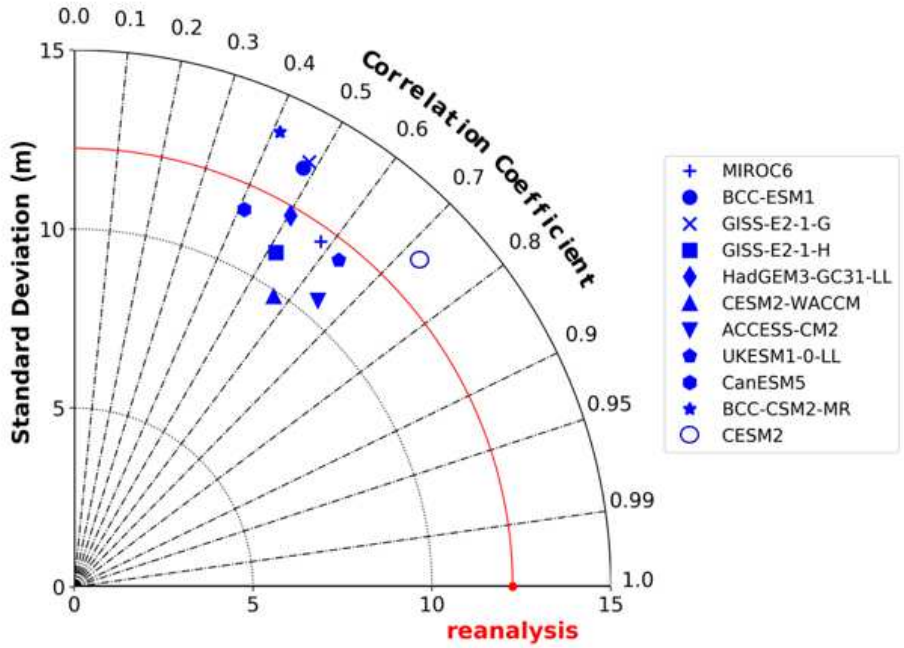

Fig. 3 Taylor diagram of the comparison of the N-S phase of the PDP (i.e., the Year +2 pattern in Fig. 1e) in the CMIP6 model output relative to that derived from the 20th Century Reanalysis. The standard deviation measure (m) is derived from the N-S index, and the correlation coefficient is computed spatially for the lag Year +2 maps from Fig. 2.

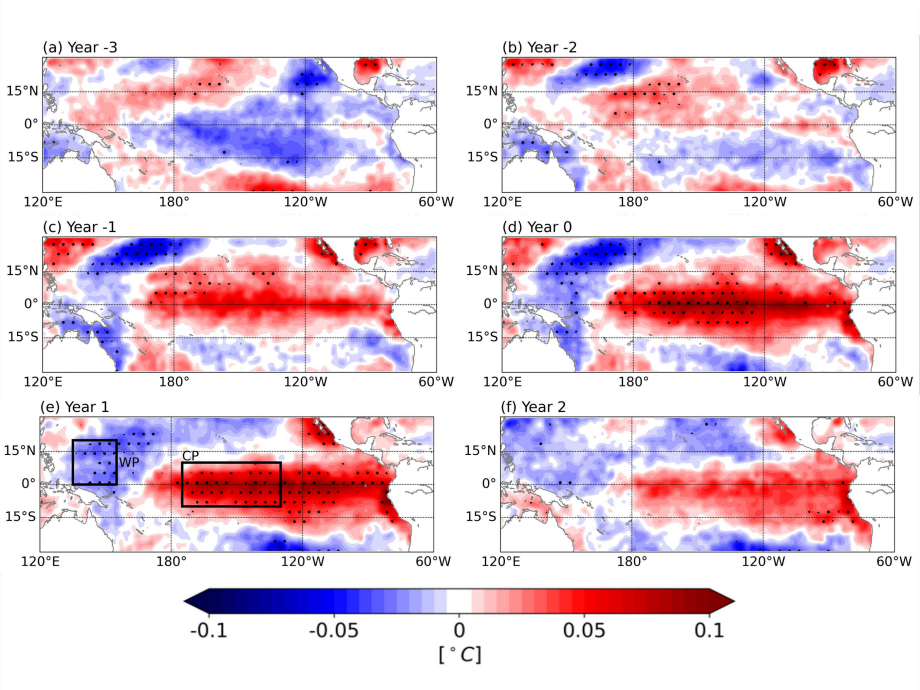

Fig. 4 Lag regression of NDJFM monthly-mean SSTa (°C) onto the PDP index from HadISST from (a) Lag Year -3 to (f) Year +2. Positive lags indicate the PDP index leads SSTa and vice versa for negative lags. Stippling denotes statistically significant ($p < 0.05$) regression coefficients found using a bootstrapping method with 5000 iterations (with replacement). Black boxes in (e) defined in text.

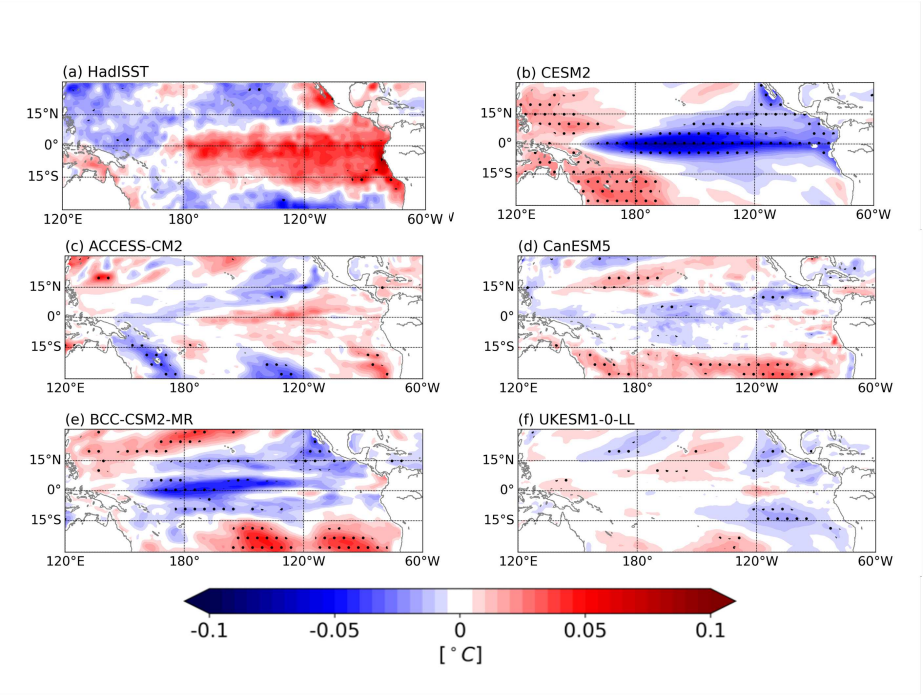

Fig. 5 (a) Same as Fig. 4e. (b)-(f) As in (a) but for the five CMIP6 models at Year +2.

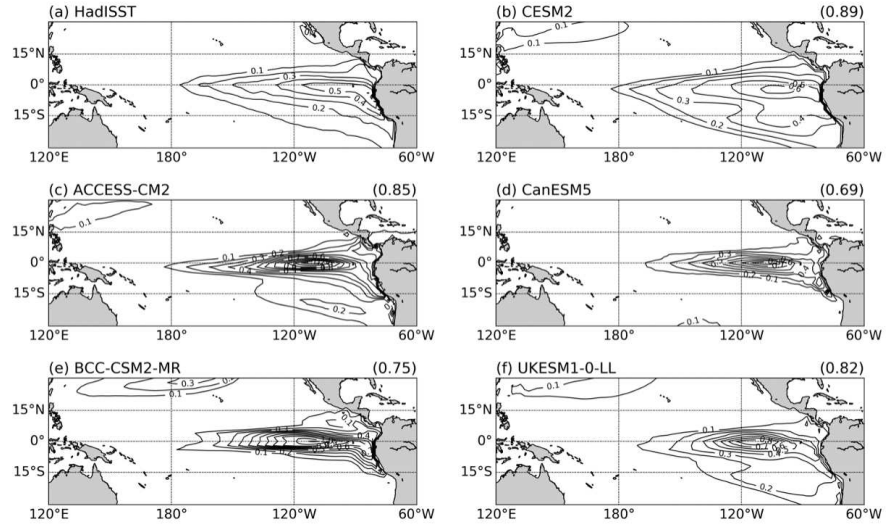

Fig. 6 Standard deviation (°C) of the leading EOF mode of monthly-mean tropical Pacific SSTa over the domain 30°S - 30°N, 120°E-60°W after removing variability associated with the Niño-4 index for lags -3 to +3 months (i.e., the canonical ENSO signature) for (a) HadISST and (b)-(f) the five CMIP6 models. Values included in parentheses in (b)-(f) are the spatial correlations of each model with HadISST results shown in (a). All correlation values are statistically significant ($p \ll 0.001$)

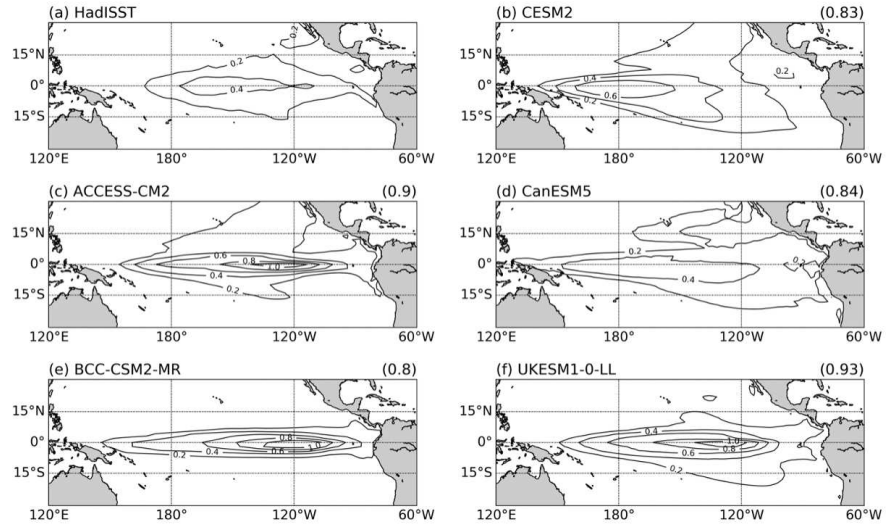

Fig. 7 As in Fig. 6 but for the CP ENSO signature (see text for details).

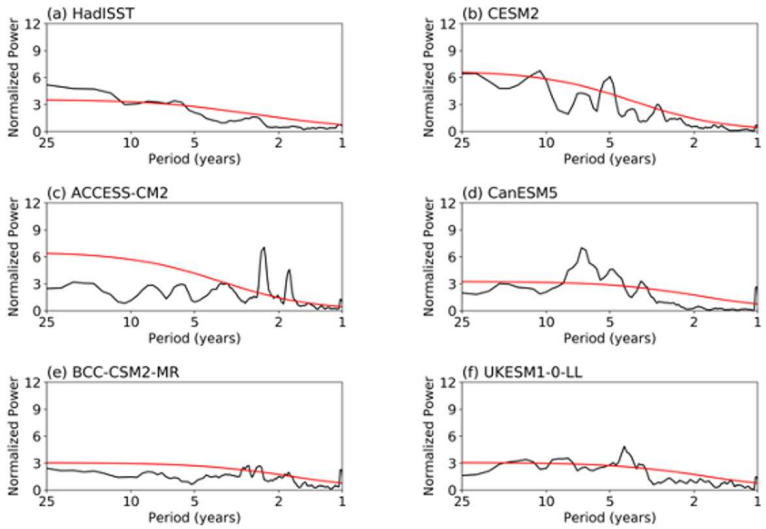

Fig. 8 (black) Power spectra of the leading principal component time series for CP ENSO (i.e., associated with the structure in Fig. 7 for (a) HadISST and (b-f) the five CMIP6 model output. (red) The 95% confidence spectrum level. Power spectrum values in all panels normalized by the total variance of the index.

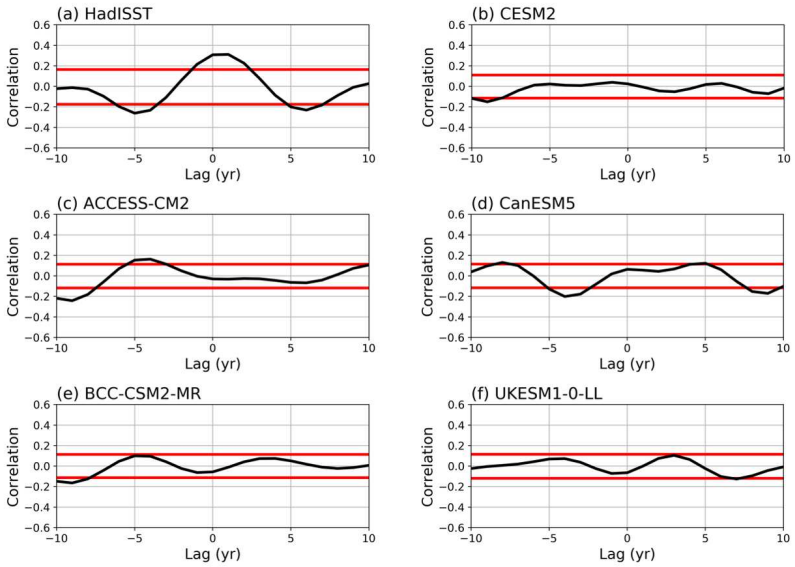

Fig. 9 (black) Lag correlation (from -10 to +10 years) of the PDP Index with the 7-20 year^{-1} band-passed NDJFM-averaged CP ENSO index for (a) HadISST and (b)-(f) the five CMIP6 models. Positive lags indicate the PDP leads the CP ENSO index and vice versa for negative lags. (red) 95% confidence interval determined from a two-sided bootstrapping method with 5000 iterations (with replacement).

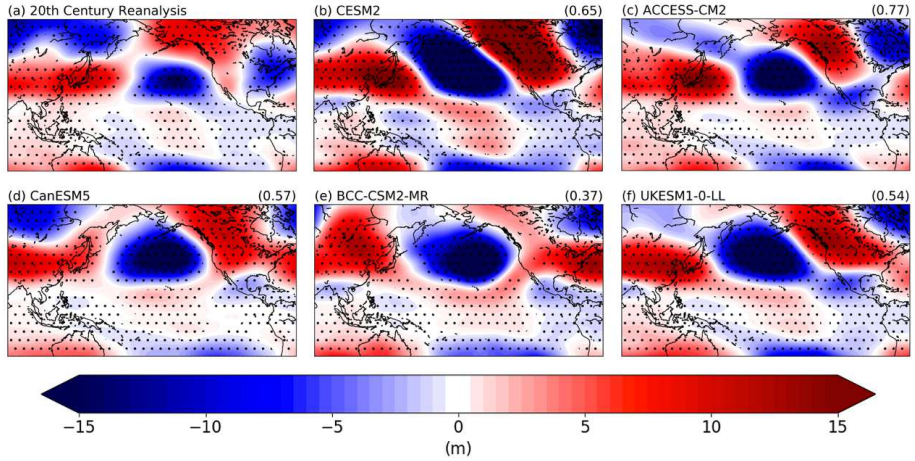

Fig. 10 Regression of 7-20 year^{-1} band-pass filtered NDJFM averaged monthly-mean eddy geopotential height anomalies (m) onto the standardized NDJFM averaged monthly mean time PDP-related SSTa pattern (see text) in (a) HadISST and (b-f) the CMIP6 models. Stippling indicates statistical significance ($p < 0.05$) using a bootstrapping method with 5000 iterations (with replacement).

Supplementary Files

This is a list of supplementary files associated with this preprint. Click to download.

- SI.tex
- history.txt